Compact time-domain diffuse optics system based on CMOS technologies for fast acquisitions of heartbeat-induced absorption changes

Elisabetta Avanzi, Tuomo Talala, Laura Di Sieno, Alberto Dalla Mora, Ilkka Nissinen, Member, IEEE, and Jan Nissinen

Abstract— This work introduces a novel compact Time-Domain Diffuse Optics (TD-DO) system based on CMOS integrated circuits for being potentially used in non-invasive tissue characterization and physiological monitoring. The system incorporates a ~800 nm emitting laser diode and a 256-channel Single-Photon Avalanche Diode (SPAD) line sensor, offering high-throughput data acquisition. It offers remarkable capabilities for non-invasive investigations of diffusive media for biological and non-biological applications. To enhance system performance, an alignment method of the TD curves based on cross-correlation maximization is proposed and validated under internationally agreed protocols, such as MEDPHOT and nEUROPt. Finally, fast oscillations in optical properties corresponding to the heartbeat have been detected, showcasing the potential of the system for real-time physiological tracking. The results display the potential of the proposed compact TD-DO system, paving the way for the implementation of wearable instruments capable of non-invasively tracking fast physiological dynamics with high accuracy and robustness.

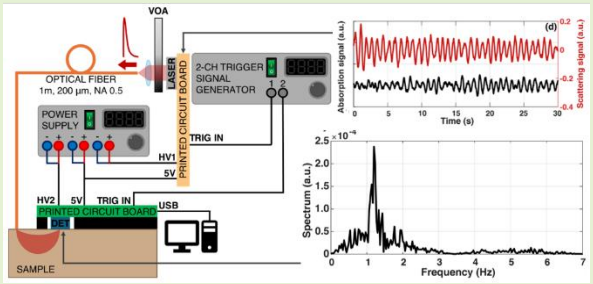

Index Terms— Single-photon avalanche diode, time-correlated single-photon counting, time-domain diffuse optics, fast measurements.

I. Introduction

TIME-Domain Diffuse Optics (TD-DO) is a powerful tool to non-invasively investigate diffusive media [1] for biological (e.g., optical mammography, brain mapping and muscle monitoring) and non-biological applications (e.g., quality assessment of fruits, wood, and pharmaceutical products) [2]. It consists of the injection of picoseconds laser light pulses into the sample and the collection of the Distribution of Times of Flight (DTOF) of the re-emitted photons by using the Time-Correlated Single-Photon Counting (TCSPC) technique [3]. Through the analysis of this signal, it is possible to retrieve the information carried by photons along their paths.

Manuscript received ….; accepted …... Date of publication …..; date of current version …..This work was supported by Academy of Finland, under Contracts 323719 and 330121." (Elisabetta Avanzi and Tuomo Talala are co-first authors.) (Corresponding author: Jan Nissinen).

Elisabetta Avanzi, Laura Di Sieno and Alberto Dalla Mora are with the Politecnico di Milano, Dipartimento di Fisica, 20133 Milano, Italy (e-mail: elisabetta.avanzi@polimi.it; laura.disieno@polimi.it; alberto.dallamora@polimi.it).

Tuomo Talala, Ilkka Nissinen, and Jan Nissinen are with the Circuits and Systems Research Unit, University of Oulu, 90014 Oulu, Finland (tuomo.talala@oulu.fi; ilkka.nissinen@oulu.fi; jan.nissinen@oulu.fi).

Indeed, depending on the microstructure and the chemical composition of the sample, photons may undergo several scattering events and, if not absorbed, can be re-emitted from different locations of the sample at some distance from the injection point, the so-called Source-Detector Distance (SDD) [4]. If the measurement is performed with a single source-detector pair in reflectance geometry (i.e., with source and detector placed on the same surface of the sample), the technique allows one to disentangle the reduced scattering coefficient (μ'_s) from the absorption one (μ_a) and to encode the mean penetration depth reached by the photons in the arrival time. As a result of these advantages, the TD approach provides significantly more informative content when compared to its counterparts, such as Continuous Wave (CW) one, while this latter is widely available on the market being based on cheaper and more compact technologies. There is therefore a tremendous interest in reducing cost and size of TD approaches. To effectively detect single photons and limit the DTOF distortion to less than 1%, the photon Count Rate (CR) is generally set between 1% and 5% of the laser pulse rate. By doing so, the effect of the pile-up distortions on the TCSPC acquisition is negligible [3]. However, this approach leads to a poor Signal-to-Noise Ratio (SNR) and a slow acquisition rate,

restricting the capability of the system to potentially track fast and deep tissue dynamics [5], [6]. The use of short SDD would enable high SNR, but the presence of slow diffusion tails in the Instrument Response Function (IRF) could hinder the information extraction from the deep layers of the medium [7]. Therefore, of particular interest would be the use of large SDD. In this case, a high SNR can be achieved by maximizing the light harvesting capability of the detector in combination with high throughput timing electronics. For this reason, in recent years, many efforts have been made to obtain advancements in the miniaturization of the devices (to directly host together sources/detectors), in the creation of large-area microelectronic detectors (to increase the total amount of collected photons), and in the development of high throughput TCSPC systems (to maximize the amount of data transferred) [8]. All these improvements allowed the detection of the heartbeat using functional Near-Infrared Spectroscopy (fNIRS) [9], [10], enabling acquisitions with SDDs from 10 up to 50 mm. The development of a fully integrated and compact (i.e., potentially wearable) system able to detect fast and deep tissue dynamics at large SDD is still missing.

Let us now examine the latest cutting-edge compact instruments reported in the literature for TD-DO. In reference [11], a stand-alone, ultra-compact device (approximately 4 cm^3) designed for multi-wavelength TD-DO is introduced. It represents the first fully integrated compact 8-wavelength time-gated DO system. The device comprises four optodes, each one consisting of: i) 8 picosecond pulsed laser diodes with various wavelengths, covering a spectral range between 635 nm and 1064 nm to effectively probe different tissue constituents; ii) a large-area (variable, up to 8.6 mm^2) fast-gated digital Silicon PhotoMultiplier (SiPM), ensuring an efficient detection of re-emitted photons; and iii) the necessary acquisition electronics to record the DTOFs. It shows an optical responsivity (i.e., DO figure-of-merit that quantify the detector light harvesting efficiency) of 1.8 × 10^{-6} m^2sr and 5.1 × 10^{-7} m^2sr at 670 and 830 nm, respectively. The 8 lasers operate at 40 MHz and acquisitions down to 5 ms are feasible. However, it has been validated only under standard CR conditions for TCSPC (almost 5% of the laser rate), therefore there is no evidence of the fact that this instrument can work in a high throughput. On the other hand, reference [10] describes a wearable whole-head.coverage TD-fNIRS system, consisting of 52 modules, arranged in a headset design. Each module is made of: i) a central dual wavelength laser source (a 690 nm and a 850 nm edge emitting laser diode); ii) six hexagonally arranged detectors; and iii) the electronics needed to perform time-of-flight measurements. It shows an optical responsivity of 7.2 × 10^{-8} m^2sr and 2.5 × 10^{-9} m^2sr at 690 nm and 850 nm, respectively. The lasers work at 20 MHz and acquisitions down to 10 ms are needed to perform spectroscopic measurement. A throughput of ~650 Mcps (median value) can be reached but at a short SDD (1 cm). Thus, the extraction of information from deep regions of the medium is limited by the slow tail in the IRF [7].

Table 1 Comparison of the system made by the 256-channel SPAD line sensor and the CMOS driver with a laser diode emitting at ~ 800 nm with state-of-the-art instruments.

	KERNEL "FLOW" [10]	**SOLUS** [11]	**THIS WORK**
Source-detector integration	Yes	Yes	Potentially available
Acquisition time per wavelength	5 ms	5 ms	10 ms
Number of wavelengths	2 (690 and 850 nm)	8 (from 635 to 1064 nm)	1 (~ 800 nm)
Optical responsivity	7.2 × 10^{-9} m^2sr (at 690 nm) 2.5 × 10^{-9} m^2sr (at 850 nm)	1.8×10^{-6} m^2sr (at 670 nm) 5.1×10^{-7} m^2sr (at 830 nm)	2.25 × 10^{-7} m^2sr (at 670 nm) ~7.20 × 10^{-8} m^2sr (at 850 nm)
Laser rate	20 MHz	40 MHz	2 MHz
SDD	3, 2 and 1 cm	Null and 2.6 cm	2 cm

The DO instrument that we are going to present in this work, instead, is made of a CMOS driver with a laser diode emitting at ~800 nm and a 256-channel SPAD line sensor [12]. Separately, their employability in DO has been validated in [8] and in [13], and their combination, presented in this work, could represent a system that has the potentiality to be wearable. The presented detection chain has an optical responsivity of 2.25 × 10^{-7} m^2sr at 670 nm, as evaluated in Ref. [8], and esteemed values of ~1.05×10^{-7} m^2sr and ~7.20 × 10^{-8} m^2sr at 800 nm and 850 nm, respectively.

The laser works at 2 MHz and in this work an acquisition time of 10 ms could be reached, even if the detector allows to reach

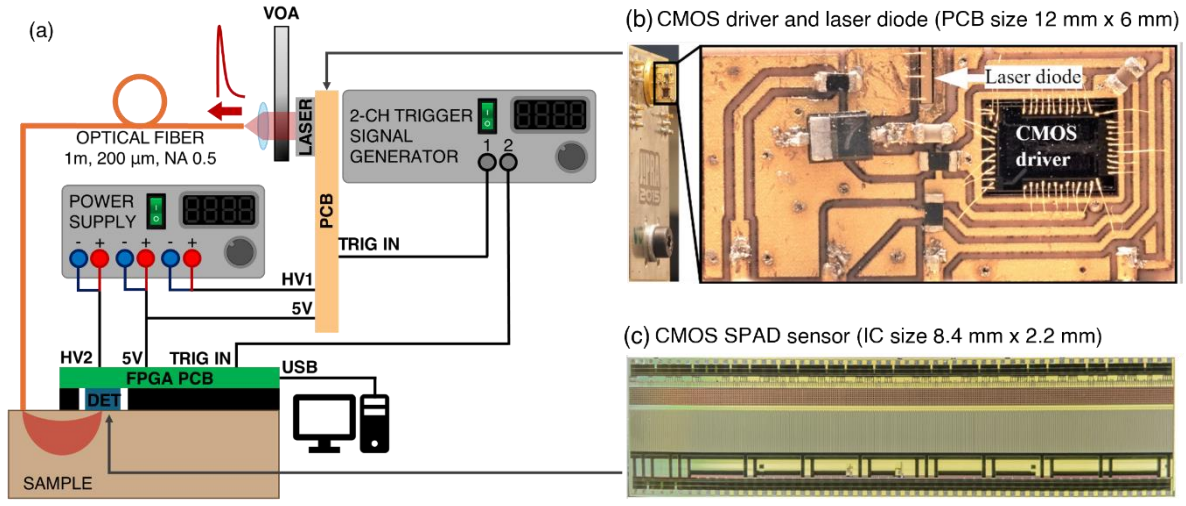

Fig. 1. a) Block diagram of the whole experimental setup. Photographs of b) the laser transmitter board and c) the CMOS SPAD sensor.

the acquisition time of a single laser event. Thanks to its high throughput, a photon count rate of ~435 Mcps have been reached at a SDD of 2 cm, and this enabled fast acquisition with suitable SNR. In the fact that this instrument can work in a high throughput. On Table 1 are summarized the main characteristics of the systems described above.

Moreover, in this work an alignment method of the DTOF based on cross-correlation maximization has been proposed and tested under internationally agreed DO protocols, namely MEDPHOT and nEUROPt [14], [15], and on in vivo measurements. Additionally, measurements on two body locations (i.e., fingertip and forehead) of one of the authors of this work in a resting-state have been performed, detecting heartbeat-induced absorption and scattering changes. To the best of our knowledge, this is the first compact pseudo-wearable instruments able to detect this pattern. We would like to stress here that our aim is to develop a compact and potentially wearable research instrument capable of being applied in measurements to observe hemodynamic oscillations in the brain during resting-state activity in humans (and not only the heartbeat effect in particular), a phenomenon gaining growing attention in the scientific and medical fields, which is essential for improving our understanding of both normal and pathological brain function [16]. Our approach focuses on designing a system that balances compactness and the ability to track these fast dynamics with high temporal resolution.

This work is organized as follows: Section II deals with the description of the system, the phantoms, the measurement protocols, and the data analysis. Section III reports the measurements results and discussion. Finally, Section IV presents conclusions and future perspective.

II. Material and methods

A. Experimental setup

The simplified block diagram of the TD-DO measurement system used in this work is shown in Fig. 1 a). A 2-channel trigger signal generator triggers a CMOS driver with a laser diode to generate an optical pulse whose power is adjusted thanks to the use of a Variable Optical Attenuator ("VOA" in Fig. 1 a)) for measurements. The optical pulse from the laser diode is coupled to a fiber after the VOA to illuminate the sample. Back scattered photons are, then, detected by a CMOS SPAD sensor placed in contact with the sample in reflectance geometry. The compact laser diode transmitter is based on a CMOS driver fabricated in 0.35 µm CMOS technology and a quantum well laser diode working in an enhanced gain switched mode [17]. The laser diode can produce energetics and short optical pulses (~100 ps) at ~800 nm when driven by 1-2 ns current pulses as described in [18]. This wavelength allows us to match the isosbestic point of hemoglobin, which we chose for this initial work as it represents the optimal balance between the two main blood absorbers. While other wavelengths in the NIR range could be used to, for example, differentiate between oxy- and deoxy-hemoglobin, the isosbestic point at 800 nm was selected for its advantages in simplifying the analysis. The amplitude of the driving current pulse of the laser diode can be adjusted by the supply voltage ("HV1" in Fig. 1 a)) so that the peak power of the optical pulse could be controlled to achieve a sufficient photon detection rate in every measurement. More details about the laser diode driver can be found in [18]. The photograph of the driver is shown in Fig. 1 b). The detector used in this experimental setup is a 256-channel CMOS SPAD line sensor [12], as depicted in Fig. 1 c). Each of the 256 channels consists of eight 27.2 µm × 27.2 µm SPADs and a 7-bit time-to-digital converter (TDC). To meet requirements of different applications, a temporal resolution, and a full-scale range of TDCs can be adjusted in ranges of 26–65 ps and 3.2–8.2 ns, respectively. In this work, a temporal resolution of 59 ps was used to obtain a full-scale range of 7.5 ns. Outputs of all eight SPADs of a channel are combined with an OR-gate so that no more than one photon can be detected by a single channel for each excitation pulse. The maximum excitation pulse rate for the detector is 2 MHz resulting in a maximum throughput of 512 million detections per second (256 × 2 MHz). Both the excitation pulse rate and the photon detection rate affect the power consumption of the detector, and the maximum power consumption is ~150 mW (2 MHz excitation pulse rate, ~100% detection probability). A much higher power consumption, ~2.5 W, is caused by the FPGA integration board (OpalKelly XEM7310-A200) that is used for data read-out and to control the detector. It should be noted, however, that only a small share of resources of the FPGA on the XEM7310 board is used in this application, and the power consumption could be reduced significantly by using a smaller FPGA chip. The CMOS SPAD sensor is triggered by the same 2-channel signal generator of the laser with an adjustable delay ("TRIG IN" in Fig. 1 a)), and an external power supply provides all needed voltages for powering the board electronics and all the SPADs ("5V" and "HV2" in Fig. 1 a)). Histograms were delivered to laptop via USB 3.0 cable. The SDD was adjusted to ~2 cm in all measurements. The choice of a 2 cm source-detector distance (SDD) is motivated by the need to capture signals from deeper tissue layers, especially in the context of brain measurements. While shorter SDDs (e.g., 1 cm) would limit the penetration depth and make it difficult to extract information from deeper layers due to the slow IRF diffusion tail introduced by our detector, larger SDDs (e.g., 3 cm) would reduce the maximum achievable count rate due to the limited detector optical responsivity. As such, the 2 cm SDD represents a proper compromise. Despite the bulky dimensions of the generator and power supply, the system has the potentiality to be employed with wearable application with appropriate modifications.

B. Data analysis

The core point of this paragraph is the temporal alignment method. Indeed, temporal drifts or fluctuations between repetitions (i.e., DTOF acquired consecutively in the same conditions to increase photon statistics and/or to compute standard deviations due to unwanted measurement variabilities) can arise due to a multitude of factors, necessitating careful consideration to ensure accurate and reliable results, especially in high throughput and high sampling rates scenarios. For instance, instability in the temporal behavior of the experimental setup, such as imperfect timing synchronization among components, can lead to temporal misalignment, causing discrepancies in the recorded data. Therefore, in this

context a crucial post-processing step involves the alignment of the signal repetitions to help to mitigate these issues effectively.

In this study, we achieved repetition alignment using a custom-made code based on cross correlation analysis (MATLAB 2023a, The MathWorks Inc., Natick, MA, USA). Cross correlation is a measure of the similarity between two signals or datasets [19]. It consists in sliding one signal over another and calculating the correlation coefficient at each step. The resulting correlation values indicate the level of similarity or correspondence between the two signals at different time offsets. Higher cross-correlation values indicate strong similarity, while lower values suggest a lack of similarity between the signals. By employing this alignment method in which cross-correlation is maximized, we ensured a high degree of similarity among repetitions, effectively mitigating potential temporal instability in the recorded data.

For each set of repetitions, we aligned all subsequent acquisitions with the first repetition of that set.

1) MEDPHOT protocol

The protocol is meant to evaluate the capability of the system in retrieving the optical properties of homogenous media [14]. The MEDPHOT kit is composed by solid phantoms based on epoxy resin with TiO_2 and black toner powders. Their concentrations are tailored to span wide range of absorption and reduced scattering coefficients.

For this study, three different phantoms were used: P1 with μ'_s = 8.15 cm^{-1} and μ_a = 0.01 cm^{-1}, P2 with μ'_s = 9.36 cm^{-1} and μ_a = 0.086 cm^{-1}, and P3 with μ'_s = 11.86 cm^{-1} and μ_a = 0.080 cm^{-1} at 800 nm. All these values have been retrieved through the characterization of the phantoms with a state-of-the-art instrument [20]. For these measurements, a SDD of 2 cm and reflectance geometry was employed.

We acquired measurements at 10 different CRs from 5×10^4 counts per second (cps) to 1.7×10^6 cps per each single TDC (which corresponds to 85% of the laser rate, thus, we are in a strong pile-up condition). The intermediate values were chosen such that, after the pile-up correction [21], their percentage with respect to the laser rate would have been equally spaced. Unless specified, all the measurements were repeated at different CRs by observing the total photon counting rate displayed by the customized read-out software, and the values reported are expressed as the percentage of the total amount of counts in the DTOF after the pile-up correction with respect to the excitation rate for a single TDC. It is worth noting that such percentage can exceed 100% as already demonstrated elsewhere [8], [21].

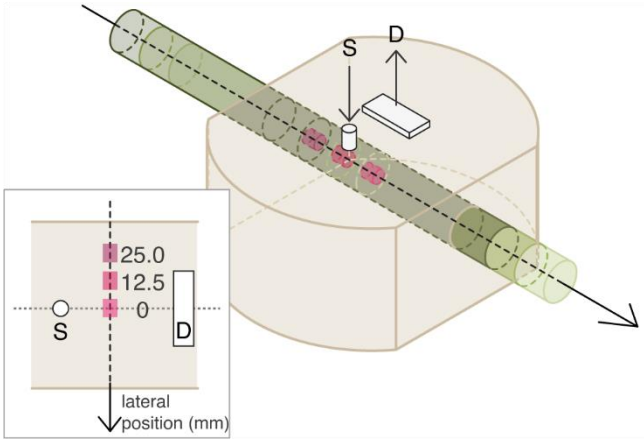

Fig. 2. Scheme of the solid switchable phantom employed in the nEUROPt phantom. Source (S) and detector (D) are placed symmetrically with respect to the rod axis, and the inclusion (small cylinder) has been moved at various lateral positions from -25 to 0 mm at steps of 2.5 mm from the source-detector pair. An insertion with a zoom of the top view geometry is shown.

For each phantom, 100 acquisitions of 10 ms each were taken. After recording the DTOFs, post-processing steps were applied to all measurements. We corrected the pile-up distortion, by using the Coates's algorithm [22], which is a simple and effective algorithm that does not require any prior knowledge of the DTOF shape and whose application in TD-DO has been systematically demonstrated in [21]. We, then, carried out Differential Non-Linearity (DNL) correction and background noise subtraction on all acquired histograms from each single TDC. These post-processing steps were separately applied to all the histograms of the TDCs. We then summed up all the DTOFs obtained from the different TDCs to generate a single histogram for each acquisition time, and we applied the alignment procedure described at the beginning of this section.

To recover the optical properties, we employed a fitting procedure based on the analytical solution of the radiative transfer equation under the diffusion approximation in semi-infinite homogenous medium in a reflectance geometry [23]. To consider the non-idealities of the system, we convolved its Instrument Response Function (IRF) with the analytical model. We fitted the curves from 20% of the peak on the rising edge down to 10% of the tail of the curve. To check the effectiveness of the aligned method, we fitted data both before and after the alignment.

2) nEUROPt protocol

The protocol allows one to evaluate the capability of the system to detect a localized absorption change buried within a homogenous medium [15]. Measurements were carried out using a switchable solid phantom specifically designed for this protocol, see [24]. It is composed by a bulk (μ_a = 0.1 cm^{-1} and μ'_s = 8 cm^{-1} at 830 nm) embedding a moving rod with a perturbation made of a 0.1 cm^3 black PVC cylinder (equivalent to a realistic inclusion of 1 cm^3 with $\Delta\mu_a$ = 0.185 cm^{-1} at 830 nm). The perturbation was able to move parallel to the top phantom surface at a depth of 15 mm. As shown in Fig. 2, we placed the source and the detector symmetrically with respect to the rod axis, and the inclusion has been moved from -25 to 0 mm (i.e., directly below the source detector pair and exactly at half of the SDD) at steps of 2.5 mm. A SDD of 2 cm and reflectance geometry was employed. The homogenous state was simulated by moving the perturbation at a lateral offset of -30 mm from the source-detector pair, so that its effect could have been considered negligible. As for the MEDPHOT protocol, 100 repetitions of 10 ms were acquired for each position of the rod. We used the same 10 CRs employed for the MEDPHOT protocol and the same post-processing steps were applied.

We evaluated the contrast (C) and the Contrast-to-Noise-Ratio (CNR). The first is defined as the relative change in the number of photon when the perturbation is present (heterogenous state) with respect to when the perturbation is absent (homogeneous state), while the second is an index of the robustness of the contrast with respect to the fluctuations of the system. They are computed as:

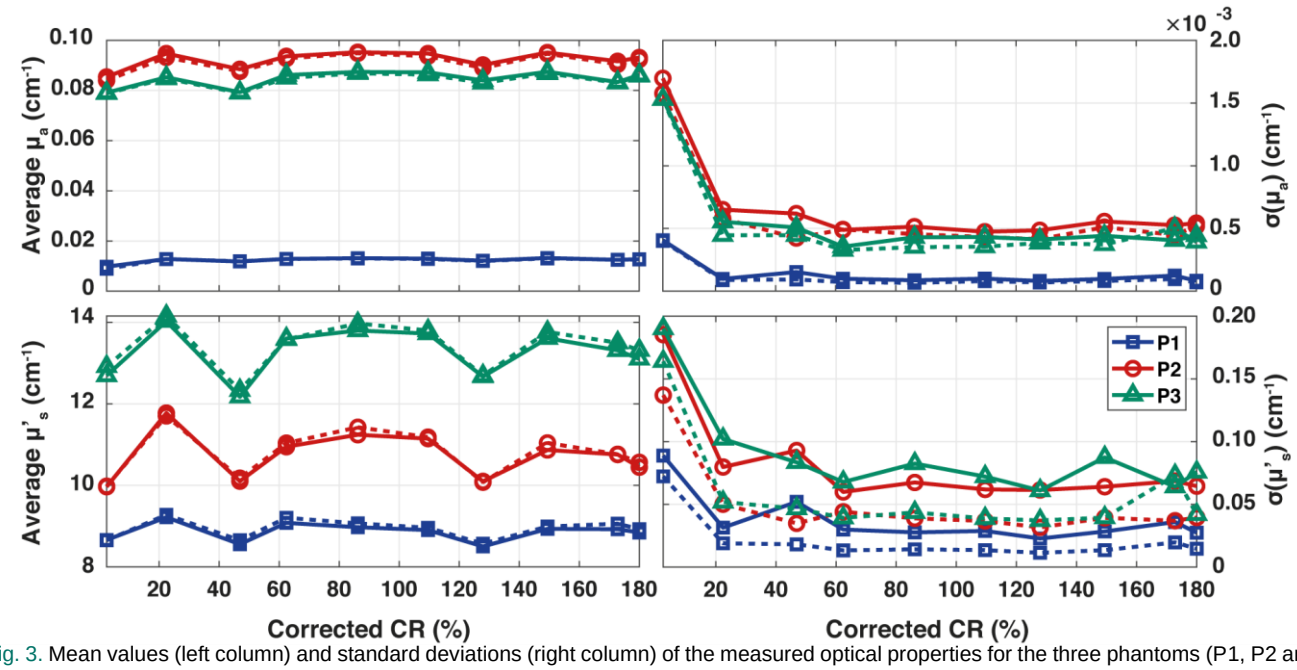

Fig. 3. Mean values (left column) and standard deviations (right column) of the measured optical properties for the three phantoms (P1, P2 and P3, see Section II B. for further details) at various corrected CR percentages. The data is presented both without (solid lines) and with (dotted lines) the alignment of the repetitions.

$$C = \frac{N_0 - N}{N_0} \quad (1)$$

$$CNR = \frac{N_0 - N}{\sigma(N_0)} \quad (2)$$

where N_0 and N are respectively the number of counts for the homogeneous and heterogenous cases, while $\sigma(N_0)$ is the standard deviation of the homogenous counts computed among all the repetitions. Starting from the post-processed curves, the contrast and the CNR were computed for 7 subsequent time-gates of 1 ns width starting 250 ps before the temporal position of the peak of the IRF, as shown in Fig S.1. of Supplementary Materials.

3) Heartbeat-induced optical changes

In this case we performed measurements at two body locations (i.e., on the fingertip in transmittance -as its size would make the measurement more sensitive to boundary effect in reflectance- and on the forehead in reflectance -as its size prevent the possibility to measure it in transmittance- at a SDD of 2 cm) to validate the suitability of this device in recording heartbeat induced absorption changes. The subject was one of the authors of this work. For each location, measurements of 30 s were acquired with an integration time of 10 ms, and a saturated CR of almost 1.7 Mcps for each TDC was set.

In terms of data analysis, we looked at the time courses of three separate signals: total counts, μ_a and μ'_s. The first was obtained by summing up all the TDC channels, while the other two were retrieved by using the same fitting procedure described in the Section II. B.1) on not aligned DTOFs. For the fingertip a homogenous medium in transmittance geometry has been considered. While, for the forehead, reflectance geometry has been used. A "filtering" approach was, then, employed to process all the signals under investigation and reduce potential artifacts (e.g., system fluctuations and Poisson noise). In particular, we began by subtracting a moving average of order 70 from the original signal to remove low-frequency trends and baseline variations (e.g. drifts of laser/detector due to temperature changes during the measurement). This step ensured that only high-frequency fluctuations remained in the signal. Next, we computed a second moving average, this time over 20 samples, to smooth the signal by reducing the effect Poisson noise, while preserving relevant features. Finally, we calculated the power spectrum for the total counts of the recorded signal, as well as for the retrieved absorption and reduced scattering coefficients. This was done using a custom-made code based on the Fast Fourier Transform (FFT) to efficiently decompose the signals into their frequency components and analyze their spectral content (MATLAB 2023a, The MathWorks Inc., Natick, MA, USA).

III. Experimental Results and Discussion

A. Performances of the system with short acquisition time and alignment

1) MEDPHOT Protocol

Fig. 3 shows the averages and the standard deviations of the retrieved optical properties (μ'_s and μ_a) for the three phantoms at different CRs without (solid lines) and with (dotted lines) the alignment of the repetitions. It is important to note that the reported CR percentage values are obtained after applying the pile-up correction. This means they can exceed 100% because the algorithm accounts for all photons that could have been potentially detected if the distortion had not occurred. Regarding the recovered mean values, the findings reveal that, in most cases, the application of alignment does not significantly improve accuracy (i.e., absolute errors with respect to expected values), as the maximum difference between aligned and not aligned data remains below 2% for the majority of CRs and for both coefficients. An exception is observed at CR = 2.5% (at the very beginning of the x-axis) for the average absorption coefficient of the phantom P1, where the difference reaches nearly 8.8% (in Table S. I within Section S.

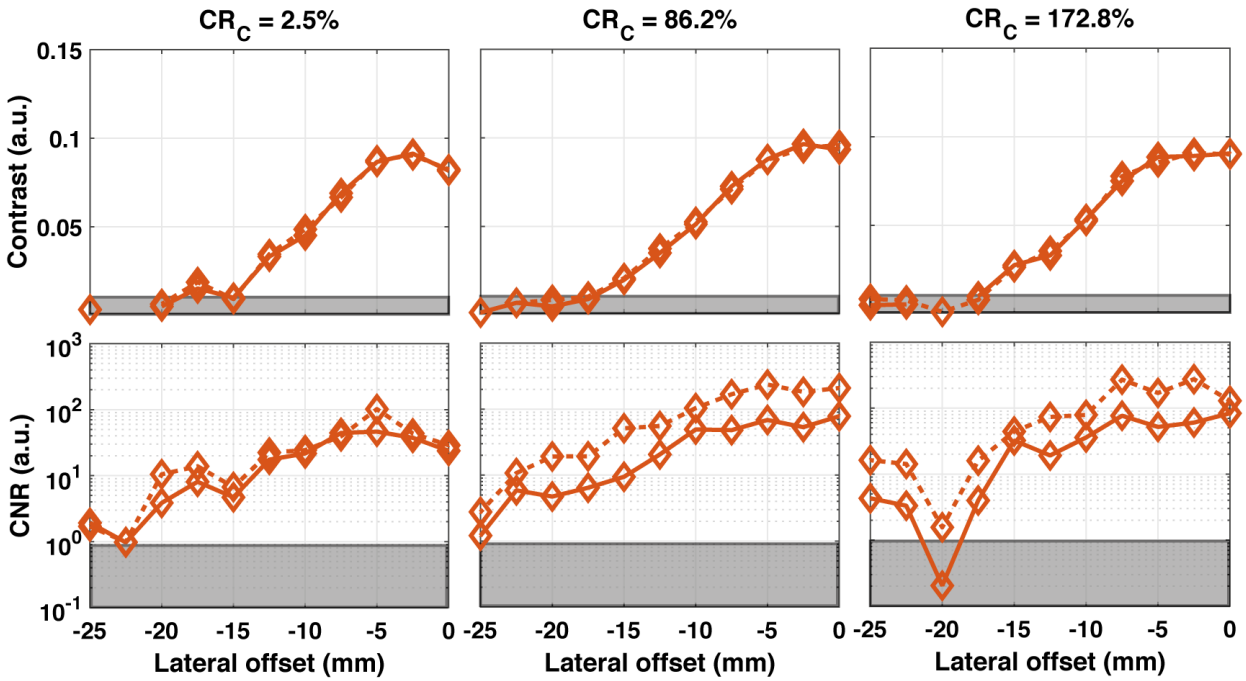

Fig. 4. Contrast (first row) and CNR (second row) at different lateral positions of the inclusion with respect to the source-detector axis for gate 2.25 – 3.25 ns. The values are reported both without (solid lines) and with (dotted lines) alignment of the repetitions. Three different photon CRs have been considered (columns).

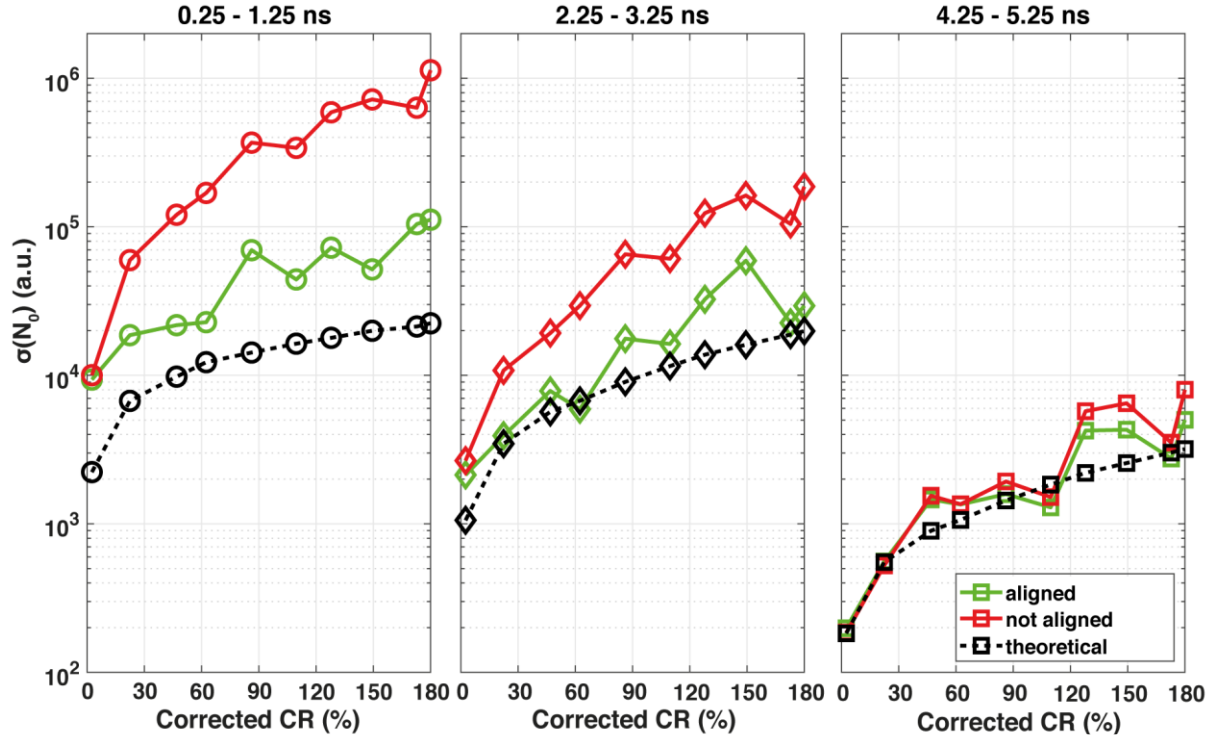

Fig. 5. Comparison of the standard deviation of the homogenous counts in three time-gates (symbols) at various corrected CR values. The values with alignment procedure applied (solid green) are reported together with the not aligned (solid red line) and the theoretical (dotted black line) ones, The graph in the middle represents data obtained for the same gate (2.25-3.25 ns) considered for Fig. 4.

I of the Supplementary Material are listed the retrieved values of the optical properties with and without the alignment procedure applied).

This discrepancy is justifiable, given the challenging task of recovering an almost negligible μ_a at a low SNR, where even minor variations in DTOF shape can influence the fitting procedure. Conversely, the alignment does demonstrate a notable reduction in standard deviation values across all samples and CRs, particularly evident in the retrieved μ_s'. For instance, for the P1 phantom, an average reduction of the

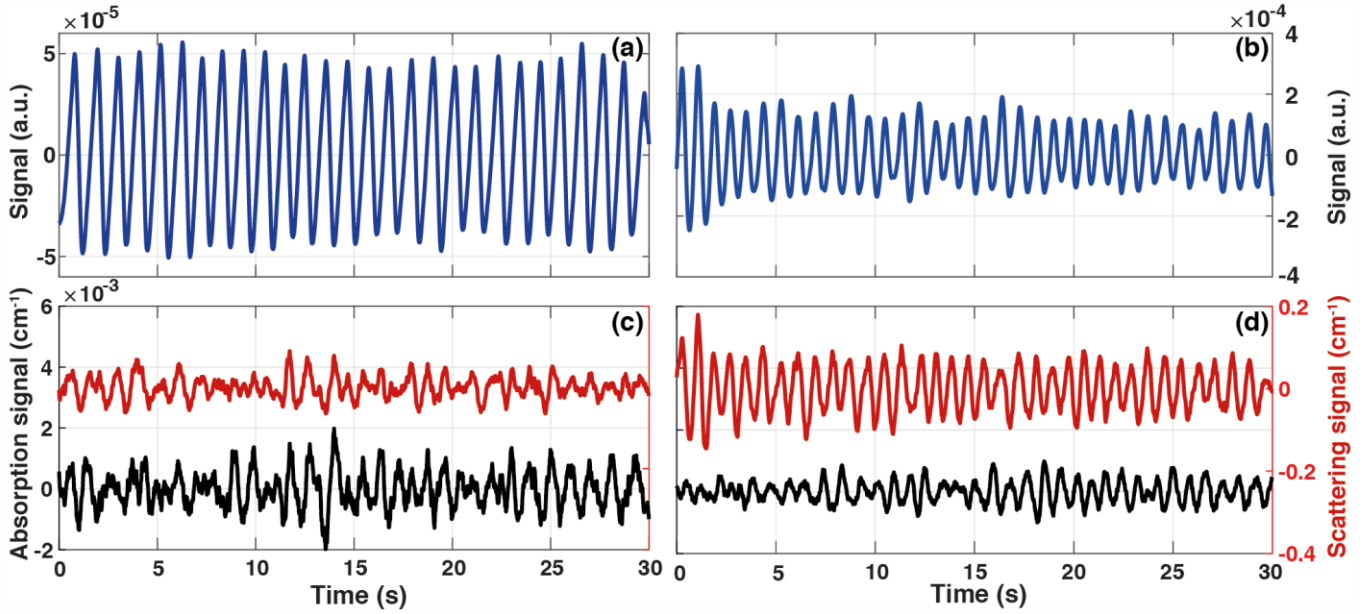

Fig. 6. Results of the resting-state measurements on the fingertip (a,c) and of the forehead (b,d): a) and b) represent the total signals recorded, after the filtering. While c) and d) show the comparison of the temporal absorption signal (black curve, left y axis) and scattering signal (red curve, right y axis), after the filtering procedure.

standard deviation of approximately 50.7% is observed for μ'_s, against the 20.8% for μ_a. This reduction in variability among repetitions indicates that the retrieved information becomes more precise and less susceptible to potential system fluctuations affecting the measurements. Overall, these findings underscore the potential of the alignment process to enhance the reliability and consistency of optical property retrieval, thus contributing to the robustness of the characterization of optical properties of homogeneous media even at short acquisition times.

2) nEUROPt protocol

Fig. 4 illustrates the contrast (first row) and the CNR (second row) calculated at different lateral locations of the inclusion for the time-gate 2.25 – 3.25 ns (symbol and color, the same as the rectangle color in Fig. S. 1. in Section S. II. of the Supplementary Material). The data are reported without (dotted lines) and with (solid lines) the application of the alignment procedure. The gray regions represent the conventional threshold below which the visibility of the perturbation is not ensured. Indeed, it is necessary to have a contrast larger than 1% (commonly and associated to physiological fluctuations induced in living tissue) a CNR larger than 1 (granting a change in counts due to the perturbation presence greater than the intrinsic fluctuations of the measurements).

As expected, higher CRs extend the lateral distance at which perturbations become visible due to increased SNR, enabling the detection of the later section of the tail of the DTOF and, generally, associated with enhanced distinguishability of perturbation at large distances [25]. To have a complete look of the contrast and CNR, it is possible to see the complete nEUROPt protocol in the Section S.II of the Supplementary Material. In particular, from the results shown in Fig. S. 2-8 it is possible to see that the maximum lateral distance at which the perturbation is visible is 22.5 mm with CR = 86.2%, with time gates of 3.25 – 4.25 ns, 4.25 – 5.25ns and 5.25 – 6.25 ns.

Regarding the contrast, it is possible to see that the alignment procedure is not affecting the retrieved values; indeed, the curves are almost overlapped for all the gates at all CRs. On the contrary, the CNR is highly affected by the alignment procedure, in particular for the gate 2.25-3.25 ns, where we assist to the CNR maximization, for all the CR shown.

Since contrast remains unchanged for most of the perturbation positions, even with alignment, the improved CNR is attributed to the reduction in $\sigma(N_0)$ as shown in equation (2). To gain further insight, let us now consider Fig. 5 which compares the standard deviation of homogenous counts at various CRs in three time-gates (symbol). Along with the not aligned values (solid red line), we report the values with alignment procedure applied (solid green line), and the minimum theoretical values (dotted black line).

The theoretical values are computed assuming Poisson Noise as the only source of fluctuations and are obtained as $k \cdot \sqrt{N_{0,NC}}$, with k index proportional to the pile-up correction introduced in homogenous counts and defined as the ratio between the number of homogenous counts in the time-gate after and before the pile-up correction (such that k is greater than 1). For further details on the complete explanation of this theoretical expression, readers are referred to see Section S. III in the Supplementary Material. It is possible to see that $\sigma(N_0)$ is drastically reduced when the alignment procedure is applied. In particular, the gates that are affected by alignment are those that also show an improvement in CNR values. In particular, the one that starts at 2.25 ns has the $\sigma(N_0)$ after the alignment much closer to the theoretical values and, indeed, it is the one that shows the maximized CNR in Fig. 5. These results provide comprehensive understanding of the impact of the alignment procedure on contrast and CNR, illuminating its role in enhancing the robustness of detection of localized absorption perturbation, particularly in higher CR scenarios and short acquisition time.

3) Heartbeat-induced absorption optical changes

In Fig. 6 a) and b) are represented the total signals recorded, after the filtering mentioned in Section II.B.3, for a resting-state measurement of the fingertip and of the forehead, respectively.

It is possible to see that a fast periodical component (compatible with the heartbeat) is present, and this is in line with the proof-of-principle shown in [8] using the same detector with a bulky laser system. Fig. 6 c) and d) show the comparison of the temporal μ_a (black curve, left y axis) and μ'_s (red curve, right y axis), after the filtering, associated to the fingertip and to the forehead, respectively. A fast periodical oscillation can be seen in the variation of the optical properties too. Indeed, let us now consider Fig. 7 where signals for the fingertip (top) and for the forehead (bottom) are reported. It is evident that a spectral component of 1.1 Hz and of 1.2 Hz is present in each measurement (since the measurements are not simultaneous, a slight discrepancy between the frequencies can be expected). Performing the same analysis on the total signal (see Fig. S. 10 a) and b) in Section S. IV. of the Supplementary Material), it is possible to note that the same spectral components are present in the total signal too, suggesting that these fast oscillations are consistent with the fast oscillation related to the heartbeat. Therefore, it is reasonable to hypothesize that these optical properties are oscillating due to physiological changes. We can also notice that the μ'_s is oscillating at the same frequency (see Fig. S. 10 c) and d) in Section S. IV. of the Supplementary Material) and, to the best of our knowledge, no other time-domain studies observed that the scattering properties were oscillating at the exact same frequency of the heartbeat. However, further investigation is required to determine the exact causes of these variations. Indeed, it may be related to a crosstalk between absorption and scattering during the fitting procedure [14]. Alternatively, it could be influenced by other effects that modify the scattering of the sample, such as the dilation of blood vessels due to blood pumping. The results using the cross-correlation method can be found in the Section S.IV of the Supplementary Material. As shown there, the differences between these methods are negligible.

Overall, the study suggests that the optical measurements taken on the body exhibit oscillations corresponding to the heartbeat, and there are changes in the optical properties associated with these physiological variations. The oscillations in the scattering coefficient may have multiple underlying causes that need to be further explored.

IV. Conclusion

In conclusion, we present the first compact (potentially wearable with the easy implementation of appropriate modifications) TD-DO system based on a CMOS chip embedding 8x256 SPADs with 256 TDCs and a compact laser driver with an ~800 nm emitting laser diode. In this context, the removal of bulky components (e.g., power suppliers) and the design of a single board containing both injection and detection parts could help to create a wearable device. It offers remarkable performances for non-invasive investigations of diffusive media. We proposed an alignment method, based on the maximization of the cross correlation between repetitions, to consider the possible temporal fluctuations introduced by the miniaturized electronics or fluctuations of the components. The alignment method enhances the robustness of the retrieval of the optical properties, even at high throughput and short acquisition times. We validate the efficiency of the alignment process on the whole system by using internationally agreed

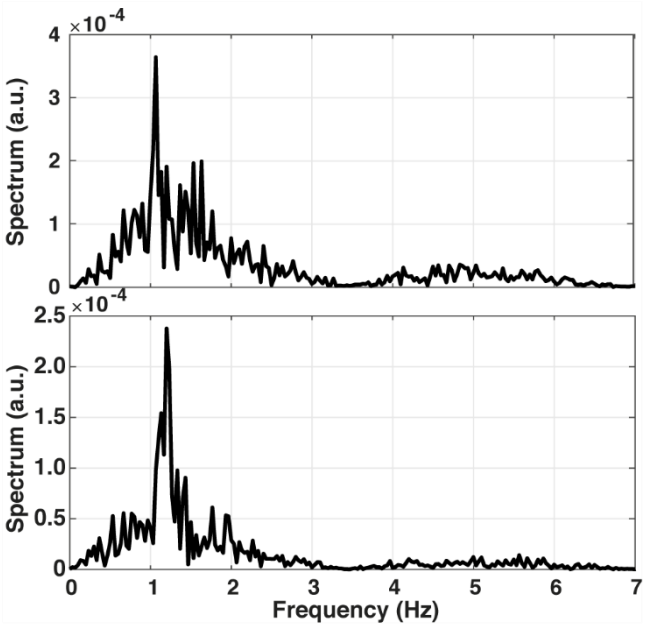

Fig. 7. Spectral components computed of the absorption signal with the FFT analysis for the fingertip (top) and for the forehead (bottom).

DO protocols (MEDPHOT and nEUROPt). In particular, the system exhibits strong potential in retrieving optical properties of homogenous media, where the variability in retrieving absorption and scattering coefficients was reduced, at maximum on average, of 20.8% on μ_a and of 50.7% on μ'_s, if alignment is present. Furthermore, once that we align the repetitions, the detection of localized absorption changes, is enhanced, and we assist to the maximization of the CNR thanks to the reduction of the fluctuations. Finally, we track heartbeat induced absorption and scattering changes in two different body locations. However, further investigations are needed to properly understand the behavior of the retrieved scattering coefficient, whose explanation, to the best of our knowledge, has not been found yet.

Furthermore, thanks to the incorporation of the alignment method directly in the FPGA, the picosecond time shifts could be immediately removed, boosting the robustness of the measurements.

These results open the way to the implementation of a compact instrument with both injection and detection electronics fully integrated and able to track fast physiological changes. For example, with the smaller FPGA chip or microcontroller with Bluetooth, the power consumption of the controller board can be decreased to ~200mW so that the total power consumption of 450 mW is achievable when the power consumption of the laser diode driver and the SPAD line sensor are 100 mW [13] and 150 mW, respectively. The Li-Po battery with a size of (10 × 34 × 51) mm^3 and a capacity of 6.8 Wh can provide 15 h operation.

ACKNOWLEDGEMENT

The authors would like to acknowledge Fondazione Bruno Kessler for designing the SPAD devices used in this work, and Alessandro Torricelli, Rebecca Re and Caterina Amendola for the useful discussions.

REFERENCES

[1] S. L. Jacques, "Time-Resolved Reflectance Spectroscopy in Turbid Tissues," 1989.

[2] A. Pifferi, D. Contini, A. Dalla Mora, A. Farina, L. Spinelli, and A. Torricelli, "New frontiers in time-domain diffuse optics, a review," *J Biomed Opt*, vol. 21, no. 9, p. 091310, 2016, doi: 10.1117/1.jbo.21.9.091310.

[3] W. Becker, *Advanced time-correlated single photon counting techniques*, vol. 81. 2005. doi: 10.1111/j.1365-2818.2006.01571.x.

[4] T. Durduran, R. Choe, W. B. Baker, and A. G. Yodh, "Diffuse optics for tissue monitoring and tomography," *Reports on Progress in Physics*, vol. 73, no. 7, 2010, doi: 10.1088/0034-4885/73/7/076701.

[5] M. B. Applegate, R. E. Istfan, S. Spink, A. Tank, and D. Roblyer, "Recent advances in high speed diffuse optical imaging in biomedicine," *APL Photonics*, vol. 5, no. 4, Apr. 2020, doi: 10.1063/1.5139647.

[6] S. Cinciute, "Translating the hemodynamic response: Why focused interdisciplinary integration should matter for the future of functional neuroimaging," *PeerJ*, vol. 2019, no. 3, 2019, doi: 10.7717/peerj.6621.

[7] D. Contini *et al.*, "Effects of time-gated detection in diffuse optical imaging at short source-detector separation," *J Phys D Appl Phys*, vol. 48, no. 4, Apr. 2015, doi: 10.1088/0022-3727/48/4/045401.

[8] L. Di Sieno, T. Talala, E. Avanzi, I. Nissinen, J. Nissinen, and A. Dalla Mora, "0.5 Billion Counts per Second Enable High Speed and Penetration in Time-Domain Diffuse Optics," *IEEE Journal of Selected Topics in Quantum Electronics*, pp. 1–11, 2023, doi: 10.1109/JSTQE.2023.3298132.

[9] R. Re *et al.*, "Reliable Fast (20 Hz) Acquisition Rate by a TD fNIRS Device: Brain Resting-State Oscillation Studies," *Sensors*, vol. 23, no. 1, Jan. 2023, doi: 10.3390/s23010196.

[10] H. Y. Ban *et al.*, "Kernel Flow: a high channel count scalable time-domain functional near-infrared spectroscopy system," *J Biomed Opt*, vol. 27, no. 07, Jan. 2022, doi: 10.1117/1.jbo.27.7.074710.

[11] L. Di Sieno *et al.*, "Smart Optode for 8-Wavelength Time-Gated Diffuse Optics," *IEEE Journal of Selected Topics in Quantum Electronics*, 2023, doi: 10.1109/JSTQE.2023.3321436.

[12] T. Talala, E. Parkkinen, and I. Nissinen, "CMOS SPAD Line Sensor With Fine-Tunable Parallel Connected Time-to-Digital Converters for Raman Spectroscopy," *IEEE J Solid-State Circuits*, vol. 58, no. 5, pp. 1350–1361, May 2023, doi: 10.1109/JSSC.2022.3212549.

[13] L. Di Sieno *et al.*, "Miniaturized pulsed laser source for time-domain diffuse optics routes to wearable devices," *J Biomed Opt*, vol. 22, no. 08, p. 1, Aug. 2017, doi: 10.1117/1.jbo.22.8.085004.

[14] A. Pifferi *et al.*, "Performance assessment of photon migration instruments: The MEDPHOT protocol," *Appl Opt*, vol. 44, no. 11, pp. 2104–2114, Apr. 2005, doi: 10.1364/AO.44.002104.

[15] H. Wabnitz *et al.*, "Performance assessment of time-domain optical brain imagers, part 2: nEUROPt protocol," *J Biomed Opt*, vol. 19, no. 8, 2014, doi: 10.1117/1.jbo.19.8.086012.

[16] L. Contini, et al. "Detectability of hemodynamic oscillations in cerebral cortex through functional near-infrared spectroscopy: a simulation study." *Neurophotonics* vol. 11, no. 03 Jul. 2024 p. 035001. doi:10.1117/1.NPh.11.3.035001

[17] B. S. Ryvkin, E. A. Avrutin, and J. T. Kostamovaara, "Quantum well laser with an extremely large active layer width to optical confinement factor ratio for high-energy single picosecond pulse generation by gain switching," *Semicond Sci Technol*, vol. 26, no. 4, p. 045010, Apr. 2011, doi: 10.1088/0268-1242/26/4/045010.

[18] J. Nissinen and J. Kostamovaara, "A High Repetition Rate CMOS Driver for High-Energy Sub-ns Laser Pulse Generation in SPAD-Based Time-of-Flight Range Finding," *IEEE Sens J*, vol. 16, no. 6, pp. 1628–1633, Mar. 2016, doi: 10.1109/JSEN.2015.2503774.

[19] S. J. Orfanidis, *Optimum signal processing : an introduction*. McGraww-Hill, 1988.

[20] F. Zhao *et al.*, "Reproducibility of identical solid phantoms," *J Biomed Opt*, vol. 27, no. 07, Feb. 2022, doi: 10.1117/1.jbo.27.7.074713.

[21] E. Avanzi, A. Behera, D. Contini, L. Spinelli, A. Dalla Mora, and L. Di Sieno, "Effects and correctability of pile-up distortion using established figures of merit in time-domain diffuse optics at extreme photon rates," *Sci Rep*, vol. 12, no. 1, Dec. 2022, doi: 10.1038/s41598-022-09385-5.

[22] P. B. Coates, "The correction for photon 'pile-up' in the measurement of radiative lifetimes," *J Phys E*, vol. 1, no. 8, pp. 878–879, 1968, doi: 10.1088/0022-3735/1/8/437.

[23] F. Martelli, S. Del Bianco, A. Ismaelli, and G. Zaccanti, *Light propagation through biological tissue and other diffusive media: Theory, solutions, and software*. 2009. doi: 10.1117/3.824746.

[24] A. Pifferi *et al.*, "Mechanically switchable solid inhomogeneous phantom for performance tests in diffuse imaging and spectroscopy," *J Biomed Opt*, vol. 20, no. 12, p. 121304, 2015, doi: 10.1117/1.jbo.20.12.121304.

[25] S. Del Bianco, F. Martelli, and G. Zaccanti, "Penetration depth of light re-emitted by a diffusive medium: theoretical and experimental investigation," 2002.

Elisabetta Avanzi received her MSc degree in physics engineering and her PhD degree in physics from the Politecnico di Milano, Milan, Italy, in 2020 and 2024, respectively. She is currently a postdoctoral research fellow at the Department of Physics, Politecnico di Milano. Her research interests include the design, validation, and application of time-resolved diffuse optical spectroscopy components and systems.

Tuomo Talala received the M.Sc. (Eng.) and D.Sc. (Tech.) degrees from the University of Oulu, Oulu, Finland, in 2018 and 2023, respectively. His research interests include the development of integrated sensors and data post-processing techniques for time-resolved optical measurements."

Laura Di Sieno was born in Varese (Italy) in 1987. She received the master's degree in electronics engineering and the Ph.D. degree in physics from the Politecnico di Milano, Milan, Italy, in 2011 and 2015, respectively. She is currently an Associate Professor with the Department of Physics, Politecnico di Milano. She has authored more than 80 papers in international peer-reviewed journals and conference proceedings. Dr. Di Sieno's activity is mainly focused on the study and application of a new approach and instrumentation for time-domain optical spectroscopy of highly scattering media using single-photon detectors.

Alberto Dalla Mora was born in Fiorenzuola d'Arda (Italy) in 1981. He received his MS degree in electronics engineering and his PhD in information and communication technology from Politecnico di Milano, Italy, in 2006 and 2010, respectively. He is currently an associate professor at the Physics Department of Politecnico di Milano, Italy. He has authored about 190 papers in international peer-reviewed journals and conference proceedings. Prof. Dalla Mora's research interests are mainly related to the development of innovative time-resolved diffuse optics techniques and instrumentation for biomedical applications.

Ilkka Nissinen (Member, IEEE) received the M.Sc. (Eng.) and Dr.Tech. degrees in electrical engineering from the University of Oulu, Oulu, Finland, in 2002 and 2011, respectively.

Since 2018, he has been an Associate Professor of analog and mixed-signal microelectronic circuit design with the Circuits and Systems Research Unit, University of Oulu. His research interests include the design of time interval measurement architecture for the integrated sensors of pulsed time-of-flight laser technologies. Dr. Nissinen has been serving as a member of the Technical Program Committee of the IEEE Nordic Circuits and Systems Conference since 2019.

Jan Nissinen received Dr.Tech. degree and Title of Docent in electrical engineering from the University of Oulu, Finland, in 2011 and 2018, respectively. He has been a Postdoctoral Researcher with the Circuits and Systems Research Unit, University of Oulu, since 2011. His research interests include designing of analog and mixed-signal integrated circuits for pulsed time-of-flight laser rangefinders, pulsed Raman spectroscopy and time-domain diffuse optics. He has designed or co-designed over 16 mixed-signal ASICs in the area of TOF laser range finding, SPAD arrays for Raman spectroscopy and miniaturized CMOS laser driver. He is PI of Academy of Finland project 2020-2024 and Business Finland project 2021-2022 focussed on the development of a single IC transceiver for time-correlated single-photon counting applications.